Proceedings of the First European Conference on Space Debris, Darmstadt, Germany, 5-7 April 1993 (ESA SD-01)

HYDROCODE MODELLING IN THE STUDY OF SPACE DEBRIS IMPACT CRATER MORPHOLOGY

J.A.M.McDonnell, D.J.Gardner, P.J.Newman

University of Kent Unit for Space Sciences,
Canterbury, Kent, England, CT2 7NR

N.J.Robertson, C.J.Hayhurst

Century Dynamics Limited, 12 City Business Centre, Brighton Road,
Horsham, West Sussex, England, RH13 5BA

ABSTRACT

The AUTODYN-2D and 3D hydrocodes have been used to study the effects of projectile density, velocity and impact angle on micrometer scale impact craters as found on NASA's Long Duration Exposure Facility (LDEF).

Unlike most experimental studies at the size and velocities considered here the calculations have concentrated on a single target material (2024 aluminium) whilst the projectile material and impact angle were varied in the velocity range 4-16km/s. This provides a much closer correspondence to the real situation encountered by orbital spacecraft such as LDEF.

1. INTRODUCTION

The return of NASA's Long Duration Exposure Facility (LDEF) provides a unique opportunity for the study of hypervelocity impact crater mechanics. Although to meteoroids the exposure geometry resulting from geocentric stabilisation provides a random impact angle, to co-orbiting space debris the exposure is deterministic. LDEF's 14 major faces permit the angular dependence to be accurately established, but the smoothing effect of 2π steradians acceptance angle for flat surface detectors prevents resolution of the fine structure of space debris in the "butterfly wings" resulting from the orbital inclination distribution. Attempts to deconvolve this smoothing have been made (ref. 1), however the fine structure is still obscured. On flat detectors we have two major physical parameters in the impact morphology (crater depth to diameter ratio and crater ellipticity) which may retain vestigial characteristics of the impact parameters. However, to decode this data it is necessary to have calibration data to which the morphology may be compared.

Experimental data at the velocities encountered by orbital spacecraft are severely limited by current laboratory acceleration techniques, and thus it was decided to study the effects of density, velocity and impact angle using computer based modelling techniques. This has the advantage that the morphology of the impact craters may be observed at any point in the calculation rather than just the end result. The initial results of this study are presented here.

AUTODYN-2D and AUTODYN-3D are interactive, integrated hydrocodes available on PC's through to supercomputers (Ref. 2). Lagrange, Euler, ALE and Shell processors are available, and can be fully coupled, in AUTODYN-2D. Currently a Lagrange processor exists in AUTODYN-3D with other processors under development.

The Lagrange processor, where the grid distorts with the material, has the advantage of being computationally fast and gives good definition of material interfaces. The Euler processor, which uses a fixed grid through which material flows, is computationally more expensive but is better suited to modelling larger deformations. Material interfaces are less well defined in Euler, so features such as crater lips are less well resolved. The ability of the Lagrange processor to simulate impact problems with large deformations can be enhanced by the use of an erosion algorithm and this is included in both AUTODYN-2D and 3D. The erosion algorithm works by removing Lagrangian cells which have reached a user-specified strain, typically 150%. In AUTODYN the user can optionally choose to discard or retain the mass and momentum of nodes associated with discarded cells. However for the purposes of this paper we chose to discard eroded nodes as previous experience showed that this tends to give better results for macroparticle impacts.

For the analyses reported here the Shock (Mie-Gruniesen) and Tillotson equations of state were used together with either the Johnson-Cook or Steinberg-Guinan strength models. All material data values used were exactly as published in references 3 to 6.

The Tillotson model was favoured since it accounts for phase changes by modelling a solid to gas transition: The Shock equation of state (EOS) does not model any phase transitions. The strength models were chosen since we wished to account for the important effects of strain and strain-rate hardening and thermal softening, including melting. Previous studies of microparticle hypervelocity impact on semi-infinite targets have tended to use a constant yield stress factored to account for strain rate effects.

2. RESULTS

2.1 Measurements and terms.

The measurement of craters and their morphology has been known, in personal experience, to add an element of confusion if the terms in use are not made clear. For the purposes of this paper, the original surface level is taken as the plane of reference, and all measurements are taken either in this plane or relative to it.

Thus, the depth of an elliptical crater is the distance between the lowest surface within the crater to the original

surface plane; the maximum diameter (D_{cmax}) is the longest line that may be measured between two opposing points on the circumference of the crater, as measured in the original surface plane; the minimum diameter (D_{cmin}) is the largest line that is perpendicular to D_{cmax} (in the reference plane).

For an elliptical crater, 2 other parameters are calculated from these values, these are termed the ellipticity (equation 1) and average crater diameter (equation 2), and are referred to as ε and D_c respectively. As can be seen, if the craters were truly ellipses rather than egg-shaped (see figs 1 and 2) ε would be the eccentricity, with D_c as the diameter of a circle enclosing the same area.

$$\varepsilon=\sqrt{1-\frac{D_{cmin}^2}{D_{cmax}^2}} \qquad (1)$$

$$D_c=\sqrt{D_{cmax}*D_{cmin}} \qquad (2)$$

2.2 Validation Calculations.

A series of analyses was used to validate AUTODYN-2D and 3D for hypervelocity impact and also to determine the suitability of processor types and material models and data for this type of problem. The Johnson-Cook strength model was used for all the validation cases described below. The validation cases were mainly concerned with impacts on semi-infinite targets to match the interests of this paper.

For microparticle impacts on semi-infinite targets, there is very little experimental data suitable for a validation study. Also existing material strength models and strength data have not been specifically derived, or sufficiently proven, for microparticle impacts. For these reasons the first study therefore concentrated on the analysis of a macroparticle at the lower velocity range (~4km/s): Macroparticle impacts for the higher velocity range (~16km/s) cannot yet be achieved experimentally. We chose to use the experimental results from Christman and Gehring (results obtained from ref. 7) since the material used for both projectile and target, aluminium 2024, is a well-characterised material, and matches the target material for the main study. Crater depths for a 4.5mm diameter, 4.5mm length cylinder impacting normally at 5km/s were calculated and compared well with experiment. As can be seen in Table 1, good agreement was obtained for the Shock and Tillotson equations of state, Lagrange and Euler processors, and AUTODYN-2D and 3D. A graphical demonstration of the agreement is seen in Figure 3 which shows the final crater profile calculated using AUTODYN-2D and 3D.

Next several analyses of microparticle impacts at the lower and higher velocity ranges were carried out and the results of these are presented in Table 2. For the marginal perforation of 4.8μm thick aluminium foil by an iron particle at 4km/s, (experiment 2 in table 2) the exit hole diameter compared well with that of McDonnell (Ref. 8).

At a late stage in the study, we obtained data published by Stradling et al. (ref. 9), for semi-infinite target impacts of microparticles. Hydrocode studies of these experiments are published in reference 10. Our study differs in one significant respect, in that we chose to model, for all cases, the effects of strain and strain-rate hardening and thermal softening. We chose to simulate iron particles impacting single crystal aluminium targets for velocities of 6.5 and 16.5km/s (experiments 3 & 4 in table 2). Since we are not aware of any suitable material strength data for single crystal aluminium we used the same data (for aluminium 2024) as for all the previous validations.

Intermediate and final crater profiles are shown in figure 4. The crater depth to diameter ratio is of interest since in the experiments the crater depth was not measured, although such a possibility exists. A very noticeable difference was found in the crater growth pattern for the two simulations and this can be partly seen in the figure: It was found that

Velocity km/s	Target Type	2D/3D Calculation	Equation of State	Euler or Lagrange	Crater Depth	Crater Diameter
5	Semi-Infinite	Experiment 1	-	-	8.4 mm	-
5	Semi-Infinite	2D	Shock	Lagrange	7.9 mm	6.9mm
5	Semi-Infinite	2D	Tillotson	Lagrange	7.7 mm	6.9mm
5	Semi-Infinite	2D	Shock	Euler	8.2 mm	8.0mm
5	Semi-Infinite	3D	Shock	Lagrange	8.3 mm	7.5mm

Table 1. cm Scale Validation Calculations.
Experiment: Al Rod [Length=4.5mm Dia=4.5mm (ref. 8)] onto semi-infinite Al target.

Velocity km/s	Target Type	2D/3D Calculation	Equation of State	Euler or Lagrange	Crater Depth (μm)	Crater Diameter
4	4.8 μm Foil	Experiment 2	-	-	-	1.44μm Perforation
4	4.8 μm Foil	2D	Tillotson	Lagrange	-	1.3μm Perforation
16.5	Semi-Infinite	Experiment 3	-	-	-	1.00μm
16.5	Semi-Infinite	2D	Tillotson	Lagrange	1.31	0. 80μm
16.5	Semi-Infinite	2D	Tillotson	Euler	2.23	1.30μm
6.5	Semi-Infinite	Experiment 4	-	-	-	1.42μm
6.5	Semi-Infinite	2D	Tillotson	Lagrange	2.15	1.31μm
6.5	Semi-Infinite	2D	Tillotson	Euler	3.11	1.65μm

Table 2. μm Scale Validation Results
Experiments: Fe Sphere [Diameters 2μm, 0.4μm and 0.8μm (experiments 2,3,4 respectively)] onto Al

the crater depth and diameter grew at a relatively similar rate in the 6.5 km/s case whereas in the 16.5km/s case the crater depth grew more rapidly at an early stage and then was virtually stationary at late stages as the crater diameter, and crater lips, carried on growing. This phenomena has been observed by others (see ref. 11), and has also been found in the main study. Figures 5 and 6 show this growth as a function of time for a spherical iron projectile at 5 and 16km/s respectively.

It is interesting to note that some impact craters found on LDEF (in particular on thermal blankets from the Ultra Heavy Cosmic Ray Experiment) bear a much closer resemblance to the crater shapes found in the intermediate stage of high velocity calculations than to a hemispherical crater shape. One explanation for these unusual craters might be the crater formation process halting before the lips expanded as far as might be expected.

Agreement between the experiment and the calculations is satisfactory, although not as close as the previous validations. The Euler and Lagrange results are respectively above and below the measured crater diameter. Likely causes for the larger differences seen in this validation are thought to be due to the use of aluminium 2024 material data and/or the use of the Johnson-Cook strength data at strain rates above the level at which the data was derived. The differences between the Lagrange and Euler results are thought to be due to the loss of energy associated with discarding eroded nodes, in the Lagrange analyses. It is possible to retain these eroded nodes, in AUTODYN-2D and 3D, and such analyses could be carried out.

2.3 Calculations

Having demonstrated the reliability of the processors in the validation calculations the main calculations were carried out. All calculations used a semi-infinite aluminium 2024 target and 1 μm diameter sphere, thus limiting the variable parameters to the impact angle, velocity and projectile material. All calculations were carried out using the Lagrange processor in AUTODYN-2D and 3D. The erosion algorithm was used and eroded nodes were discarded for consistency with the validation calculations.

Within the limited availability of high strain rate material data as wide a range of projectile densities were used. As natural particles of cometary origin are expected to have low densities it was desired to have a large set of data for low density particles. This presented the problem that few metals have a density lower then aluminium, and of these, the only one for which material data was available was Beryllium. To expand the low density set, shock data for porous aluminium was located (ref. 3), however no strength data was available. The calculations for porous aluminium were therefore performed using the same yield strength model as for aluminium 2024. These materials thus have an "artificial" yield strength model, which is expected to be stronger than that for the real material. Where possible the Johnson-Cook strength model was used, but to provide a broader range of materials the Steinberg-Guinan model was used for some of the 16km/s calculations: The Steinberg-Guinan model was not used at 4km/s since previous experience of the authors and others has shown this model to be too strong at lower velocities. The Shock equation of state (EOS) was used for the porous aluminium. The Tillotson EOS was used for other materials except where such data was unavailable and then the Shock EOS was used.

2.3.1 Projectile Density Effect.

To study the effect of projectile density on the depth to diameter ratio, AUTODYN-2D calculations of normal impacts were carried out, at 4 and 16 km/s. The results of the calculations are shown in figure 7. This shows that a reasonable straight line correlation can be fitted to the depth/diameter ratio versus projectile density data. As expected the slope of the line is lower for 16km/s, (being 0.18), than for 4km/s, (0.59). If the porous aluminium is excluded from the straight line fit, the slope is 0.57 for 4km/s.

2.3.2 Projectile Velocity Effect.

The effect of projectile velocity can be seen in figure 8. Depth/diameter ratios are plotted for several materials at 4 and 16km/s, also at 12km/s for tungsten and for a range of intermediate velocities for an iron projectile. As expected there is an apparent convergence of the depth/diameter ratios at higher velocities. But further data for intermediate velocities and higher velocities would be needed to clearly establish any convergence. It is interesting to note however that the data for iron shows a constant ratio up to 12km/s before reducing at higher velocities, whereas tungsten shows a marked reduction at 12km/s compared to 4km/s. Additional data for intermediate and higher velocities would be required to study this convergence behaviour further, which appears to be different for different materials.

2.3.3 Impact Angle Effect

To study the effect of impact angle calculations were performed using AUTODYN-3D. As with the 2D calculations the target was semi-infinite aluminium 2024, and the projectile was a 1μm diameter aluminium 2024 sphere, at velocities of 4 and 16km/s. All calculations used the Tillotson EOS and the Johnson-Cook strength models. To maintain consistency with the other 3D calculations, the normal impact case was also calculated in 3D. The result was a somewhat larger crater than the 2D, the difference being caused by lower mesh densities used for the 3D calculation (a 2D calculation with the same mesh density as the 3D calculation produced a crater much closer to the 3D result).

Figures 9 and 10 show the variation of crater sizes with impact angle for 4 and 16km/s respectively. Normalised measures of crater size are shown against impact angle in figures 11 to 13. The normalised values shown are respectively average crater diameter, crater depth to diameter ratio and ellipticity; also plotted with the ellipticity is the ratio of minimum to maximum crater diameters (D_{cmin}/D_{cmax}). The depth to diameter ratios show a relatively smooth reduction with increasing impact angle, with the ratio remaining consistently higher for the higher velocity. Figure 11 shows that the average crater diameter shows little change from 0° to 60° and then shows a marked reduction at higher angles. This nearly constant value is due to the increasing maximum diameter being compensated for by the decreasing minimum diameter. The transition from this relatively constant average diameter to a much lower value can be seen clearly in the data for ellipticity. The foregoing indicates a "critical" angle of 60° for 4km/s and 65° for 16km/s and this corresponds to large changes in slope for the minimum crater diameter (as shown in figs 9 and 10). Above 70° there is a rapid decrease in the maximum crater diameter evident in the calculations for 4km/s, but as

yet we have insufficient data to identify where this occurs for impacts at 16km/s. Figure 14 shows the elliptical crater produced by a 16km/s impact at 70°.

Detailed examinations, including animated sequences, of the analysis results were conducted from which we have observed three regimes of penetration behaviour. Our results show that up to 50-60° virtually all the projectile kinetic energy contributes to target deformation. At high impact angles, in excess of around 75° at 4km/s, from our limited analyses in this range we have observed that the projectile "ricochets" from the target. Our definition of "ricochet" here is that the projectile emerges virtually intact from the crater and that relatively little projectile energy contributes to crater deformation. In the third regime, at angles between 50° and 75° there is a transition between the two above regimes. The critical angle referred to above (60° for 4km/s, 65° for 16km/s) corresponds to the angle at which there is a rapid change in this behaviour.

3. CONCLUSIONS

The effects of projectile density, velocity and impact angle on micrometer scale impact craters have been studied using the AUTODYN-2D and 3D hydrocodes. A notable feature of this study has been the use of material models which account for phase changes, strain and strain-rate hardening, and thermal softening effects. AUTODYN-2D and 3D were firstly validated for normal impacts of centimetre and micrometer scale impacts for velocities from 4 to 16.5km/s, although there was very little experimental data which we were able to compare with for the micrometer scale impacts. All subsequent calculations considered 1μm diameter spherical projectiles impacting on semi-infinite aluminium targets at velocities from 4km/s to 16 km/s.

For normal impacts we studied the effects of projectile density and impact velocity on crater size and shape. The dependence of crater depth to diameter ratio on projectile density decreases with increasing velocity. If a linear power law relationship is assumed our results show that $T_c/D_c \propto \rho^{0.56}$ at 4km/s and $T_c/D_c \propto \rho^{0.18}$ at 16km/s. The results of the velocity dependence study show a convergence of depth to diameter ratio at increasing impact velocity. Further work is required to obtain the variation for more materials and also at higher velocities.

In the study of impact angle affect we have observed a smaller variation in the crater depth to diameter ratio for the higher velocity case of 16km/s. We have observed three different regimes of oblique penetration behaviour in the cases studied. For 0° to 50° virtually all of the projectile kinetic energy contributes to target deformation, and above approximately 75° ricochet is observed. In between these two regions there is a transition in behaviour. In this transition region there is a critical angle at which there is a rapid change in this behaviour, and this was observed to be higher at the higher velocity. This critical angle is most clearly observed in a marked change of crater ellipticity.

The study to date has demonstrated the value of hydrocode modelling in the determination of impact crater morphology . Additional work in this area would help in a further understanding, and data, which should assist in decoding craters observed on orbital spacecraft such as LDEF.

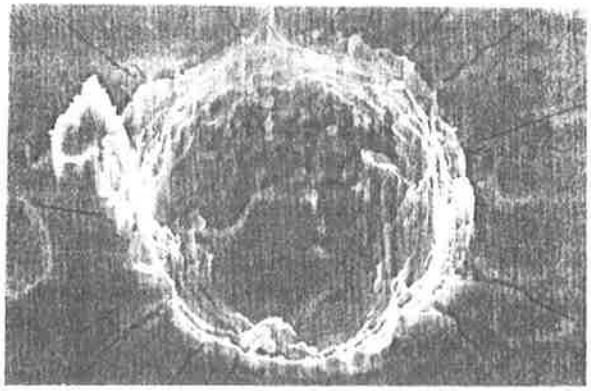

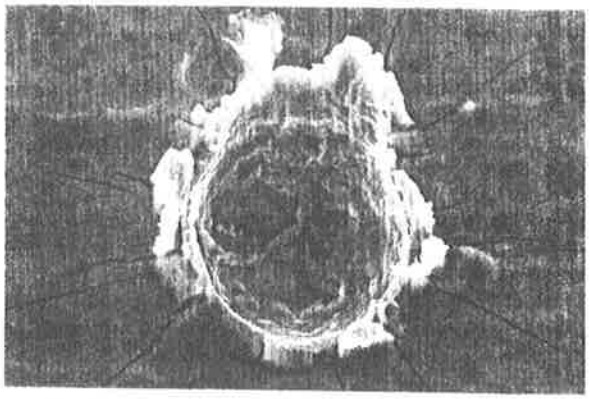

Figures 1 and 2 .Scanning Electron Microscope images of typical hypervelocity impact craters found on LDEF.

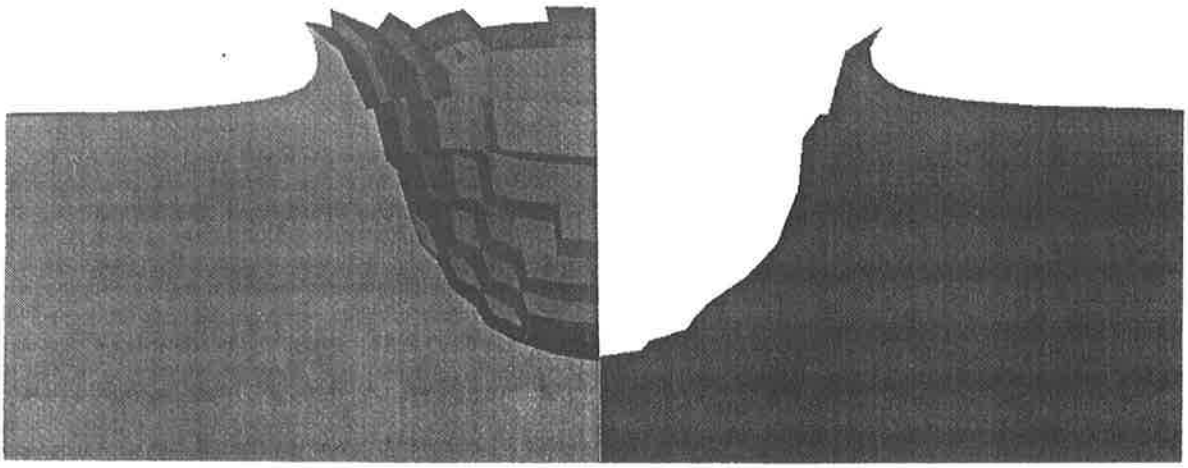

Figure 3. AUTODYN-2D (right) and 3D (left) results for macro-particle validation calculation.

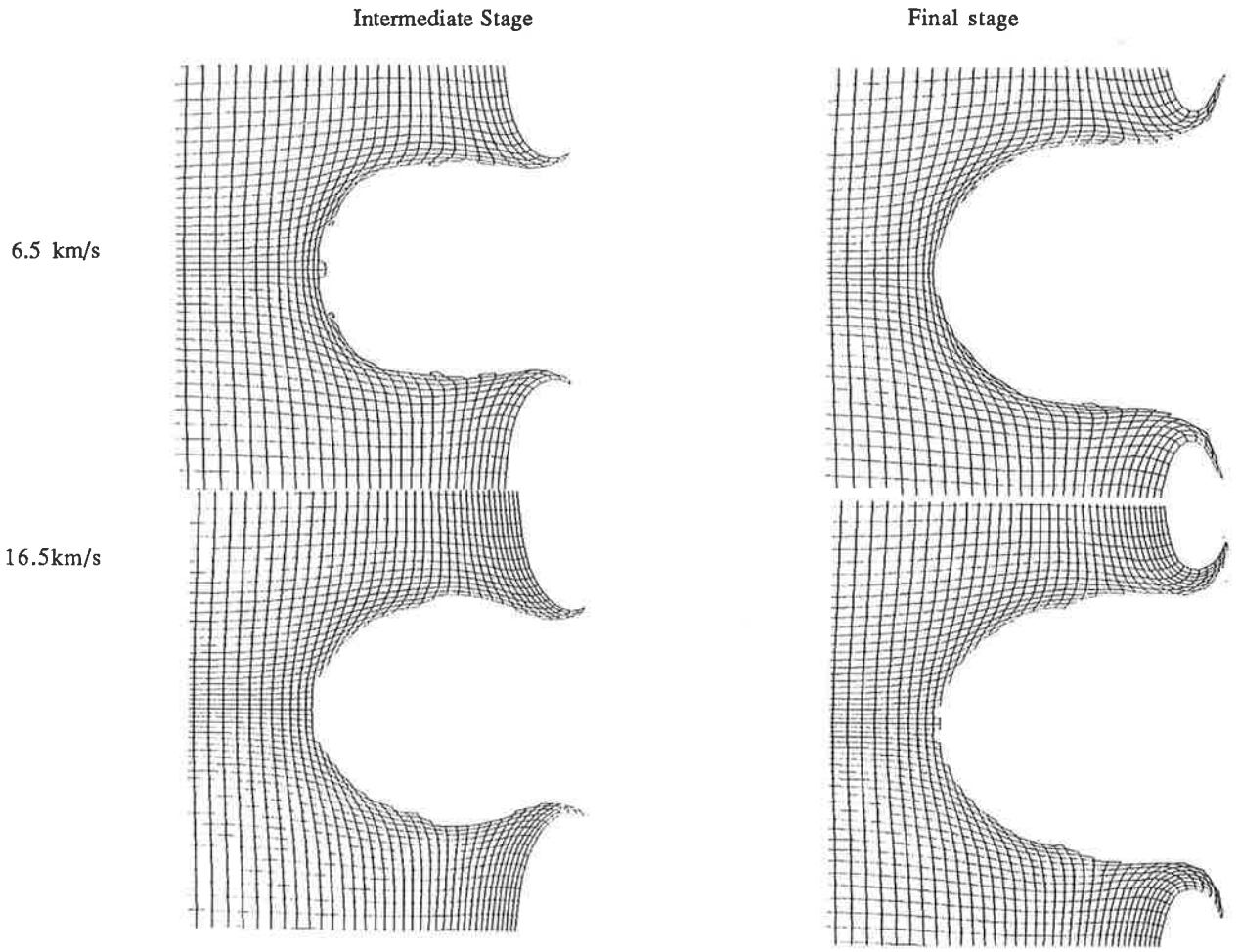

Figure 4. Intermediate and final crater shapes for aluminium projectile impacts at 6.5 and 16.5 km/s. For both impacts the intermediate time is 1/4 of the final time. The 16.5 km/s crater continues to widen after the depth is firmly established, whereas for the 6.5 km/s crater both measurements reach their final values at similar times.

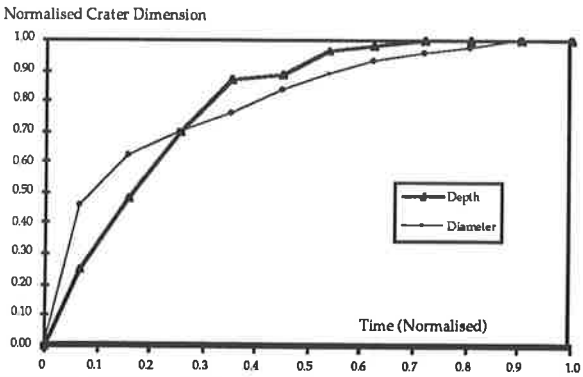

Figure 5. Crater growth curve for impact of iron projectile at 5km/s.

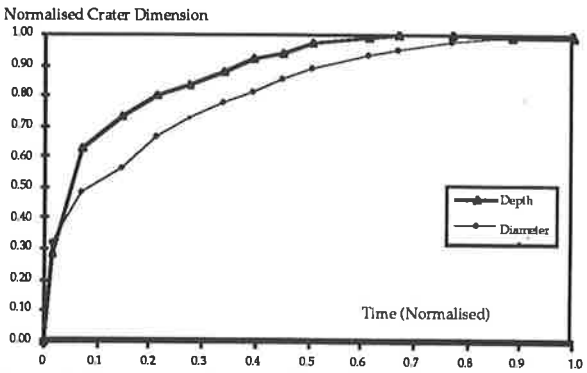

Figure 6 Crater growth curve for 16 km/s impact.

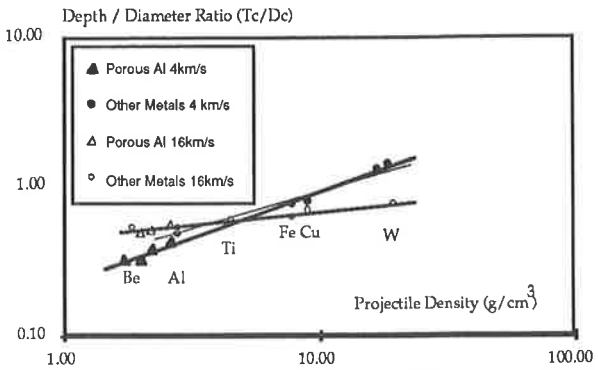

Figure 7 Effect of density on depth/diameter ratio for normal impacts at 4 and 16 km/s

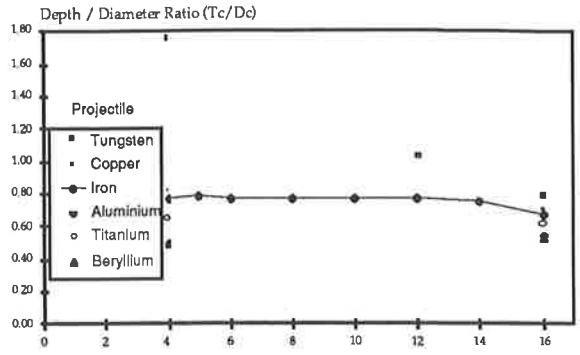

Figure 8 Velocity effect on depth/diameter ratio for a variety of projectile materials

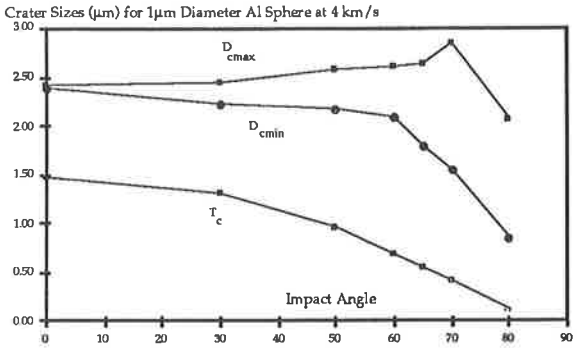

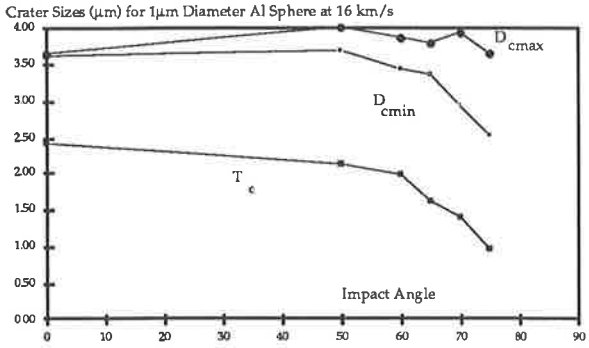

Figure 9 (left) and 10 (right) . Effect of impact angle on crater measurements at 4 and 16 km/s

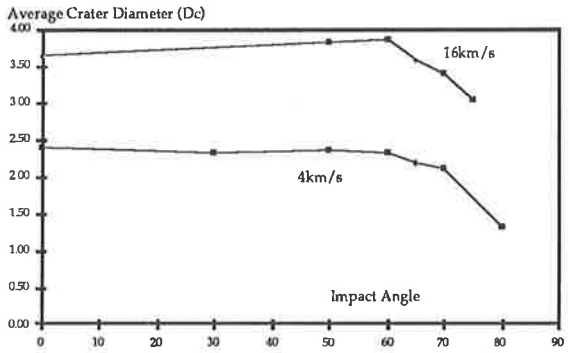

Figure 11. Impact angle effect on average crater diameter.

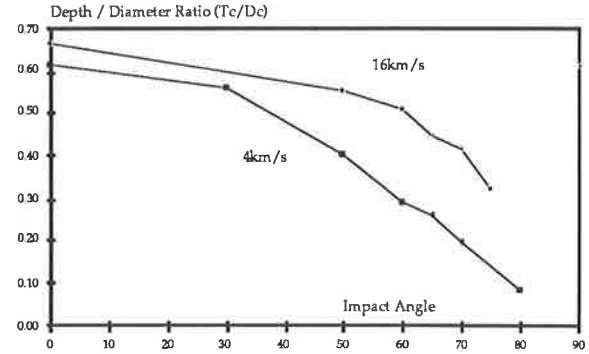

Figure 12. Impact angle effects on depth/diameter ratio at 4 and 16km/s.

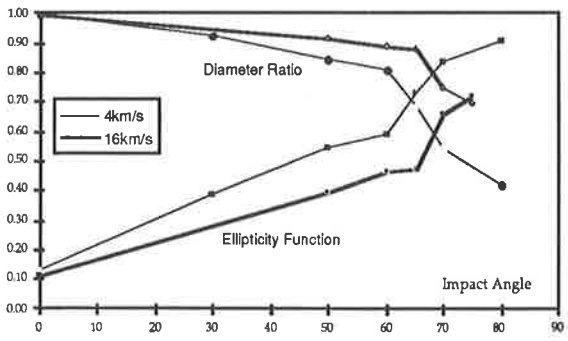

Figure 13. Impact angle effects on Crater Ellipticity. The bottom two traces show the ellipticity function, the top two are the ratio of minimum to maximum diameters.

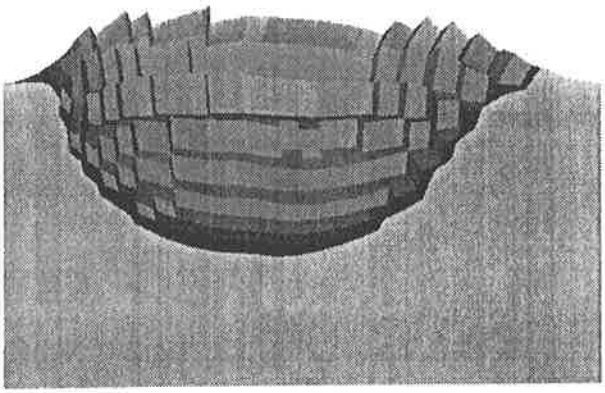

Figure 14 End result from AUTODYN-3D calculation of 16km/s impact at 70° (Cross section).

REFERENCES

1. Neish, M.J., McDonnell, J.A.M., and Niblett, D.H., Angular Distribution of The Flux of Microparticles Incident on the Surface of The Long Duration Exposure Facility, *Hypervelocity Impacts in Space*, Editor J.A.M.McDonnell, University of Kent at Canterbury, 1992

2. Cowler, M., et al. AUTODYN - An Interactive Non-Linear Dynamic Analysis Program for Microcomputers through Supercomputers, *9th International Conference on Structural Mechanics in Reactor Technology,*, Lausanne Aug.1987.

3. Group GMX-6, Selected Hugoniots, *Los Alamos Scientific Lab. LA-4167-MS* May 1969.

4. Tillotson, Metallic Equations of State for Hypervelocity I4mpact , *General Atomic SanDiego GA-3612,* July 1962.

5. Steinberg, Equation of State and Strength Properties of Selected Materials, *Lawrence Livermore Nat. Lab, UCRL-MA-106439,* Feb. 1991

6. Johnson and Cook, A Constitutive Model and Data for Metals Subjected to Large Strains, High Strain Rates and High Temperatures, *Proc. 7th International Symposium on Ballistics,* The Hague, 1983

7. Anderson, et al, A Penetration Mechanics Database, *SouthWest Research Institute, 3593/001* San Antonio

8. McDonnell J.A.M. and Sullivan, K., Hypervelocity Impacts on Space Detectors: Decoding the Projectile Parameters, *Hypervelocity Impacts in Space,* Editor J.A.M.McDonnell, University of Kent at Canterbury, 1992

9. Stradling et al., Ultra-High Velocity Impacts: Cratering Studies of Microscopic Impacts from 3 km/s to 30 km/s, *Los Alamos Nat. Lab. LA-UR-92-3811,* Nov. 1992

10 Wingate et al., Models of High Velocity Impact Phenomena, *Los Alamos Nat. Lab. LA-UR-92-1982* , Nov. 1992

11 Watts, A et al., Dimensional Scaling for Impact Cratering and Perforation, *POD Associates Inc.*, March 1993.